Fractal structure of the magnetic field in the laminar zone of the Dynamic Ergodic Divertor of the Torus Experiment for Technology-Oriented Research (TEXTOR-94)

S. S. Abdullaev,[a] Th. Eich, and K. H. Finken
Institut für Plasmaphysik, Forschungszentrum Jülich GmbH, EURATOM Association, Trilateral Euregio Cluster, D-52425 Jülich, Germany

(Received 15 January 2001; accepted 22 March 2001)

Magnetic field properties at the plasma edge in the Dynamic Ergodic Divertor (DED) for the Torus Experiment for Technology Oriented Research (TEXTOR-94) [Fusion Eng. Des. **37**, 337 (1997)] have been studied. This is done by using a generalized symplectic mapping method of integration of field line equations. It is shown that by the radial shift of the resonant magnetic surfaces implemented by change of the plasma current (or the toroidal field) one can strongly vary the plasma edge regimes from the ergodic zone dominated one to the laminar zone dominated regimes in which the field lines with short wall to wall connection lengths are predominant. The embedded in the laminar zone narrow ergodic zones have fractal structures which are investigated in detail. The fractal structures of the magnetic footprints on the divertor plate are also studied. © *2001 American Institute of Physics.* [DOI: 10.1063/1.1371954]

I. INTRODUCTION

The Torus Experiment for Technology Oriented Research (TEXTOR-94) device is being opened in 2001 to install the coils for the Dynamic Ergodic Divertor (DED) (see Ref. 1). Similar to the ergodic divertor for Tore Supra (see, e.g., Refs. 2–4) the main goal of the DED is the control of the plasma edge and the plasma–wall interaction by help of external magnetic field perturbations. The coil set will be located inside the vessel at the high field side (HFS), allowing a perturbation current to flow helically parallel to the magnetic field lines within the plasma boundary. The superposition of the perturbation field and the equilibrium field of the plasma creates an ergodization of the magnetic field lines at the plasma boundary. This should strongly affect particle transport within the ergodized zone. However, ergodic divertor experiments in Tore Supra have shown that the effect of the resonant perturbation field on particle transport was much stronger than anticipated from the estimations based on the stochastic description of transport processes in the ergodic magnetic field (see Refs. 2–4). This phenomenon gave evidence of the existence of a so-called laminar zone at the outer region, located between the ergodic zone and the plasma wall. Its main feature is, that the field lines there have shorter connection lengths, only a few poloidal turns from wall to wall, whereas the chaotic field lines in the ergodic zone do have much longer connection lengths.

First modeling efforts of the DED-TEXTOR presented in Refs. 5–17 have shown that the relative radial extensions of the laminar and the ergodic zones at the plasma edge strongly depend on the plasma parameters (plasma β_{pol}, the plasma current I_p), as well as on the divertor current. Particularly, it was found that the increase of the divertor current (or decrease of β_{pol}) does not necessarily lead to a growth of field line diffusivity, which is proportional to the particle diffusion coefficient (see Refs. 11 and 12). Due to its expected effects on the transport in the plasma edge and power load to the wall elements, the structure of the laminar zone has extensively been investigated in Refs. 6,9,10,14–17. To calculate the resulting magnetic field by applying the DED perturbation field, the Gourdon code (field line tracing) has been used. This code allows one to study the laminar zone as well as the structure of the ergodic zone, but it is not accurate enough to trace field lines a few dozens of toroidal turns and is, therefore, not a convenient way to visualize fractal structures within the perturbed magnetic edge (Refs. 5,13).

This work is devoted to the study of detailed structures of the laminar zone of the DED of the TEXTOR-94. In particular, we study a variation of the ergodic and the laminar zone induced by shifts of the spatial position of the resonant magnetic surfaces at the plasma edge, a fractal property of the laminar zone. The study is based on asymptotic and mapping methods developed in Refs. 11 and 12 for the models of the circular tokamak plasma and the ideal configuration of the divertor coils. This approach describes well the main features of the external resonant magnetic field and formation of the ergodic zone at the plasma edge obtained by Gourdon code simulations in Ref. 5. The methods are based, first, on the Hamiltonian formulation of magnetic field line equations and, second, on solving them using a new mapping method that has recently been developed in Refs. 11 and 18. The mapping procedure always conserves the main flux-preserving property of the magnetic field, unlike the Gourdon code, which violates this property at short distances while integrating the field lines equations in the zone of chaotic field lines using the conventional Adam's integration scheme. The computationally fast and flux-preserving mapping approach allows one to study detailed fine structures of

[a]Electronic mail: s.abdullaev@fz-juelich.de

the laminar zone with machine accuracy. Comparing the new approach with the former studies on the laminar zone in Ref. 15, the new model has the capability to uncover and interpret the fractal structures of the laminar zone. However, the new method uses analytical descriptions of the magnetic perturbation and the equilibrium field instead of the highly accurate numerical models used for both in the earlier approach.

One should emphasize that the magnetic field lines in the ergodic divertor device represent an open dynamical system possessing chaotic scattering properties (see Refs. 19–22 and references therein). Therefore one should expect fractal properties of field lines at the plasma edge. In poloidal divertor tokamaks the fractal structures of field lines have been studied in Refs. 23–28. Particularly, so-called tokamak divertor maps in Refs. 26–28 and the separatrix maps in Ref. 25 were employed to this behalf. Fractal properties of field lines in the DED have first been shown in Ref. 7 for the cylindrical model and later in Ref. 12 for the toroidal model of the DED. However, in the latter publications this property of field lines were not thoroughly investigated which would otherwise have revealed the fine structure of the laminar zone.

The contents of the paper is the following. The models of the plasma and the divertor coils used in the study are described in Sec. II. The Hamiltonian formulation of magnetic field line equations for these models is presented in Sec. III. The main formulas of the recently developed mapping method to integrate Hamiltonian equations are also recalled therein. The structures of the ergodic and the laminar zones are studied in Sec. IV. Particularly, we have investigated the spatial shift of the resonant magnetic surfaces, the change of the ergodic and laminar zones and field line diffusivity by the variation of the plasma current. The fractal structures of the laminar zone and the magnetic footprints on the divertor plate are studied in Sec. V by plotting contour plots of areas of field lines connecting the wall to the wall in different poloidal turns. The results are summarized and discussed in Sec. VI.

II. MODELS FOR THE PLASMA AND THE DIVERTOR COILS

We consider a model of the tokamak plasma equilibrium with nested, circular magnetic surfaces studied in Refs. 29,11,12. Let (r,θ,φ) be toroidal coordinates. The equilibrium magnetic field $\mathbf{B}(r,\theta)$ is determined by its toroidal,

$$B_\varphi(r,\theta)=\frac{\mu_o I_\varphi}{2\pi R_0(r)(1+\varepsilon\cos\theta)}, \tag{1}$$

and poloidal,

$$B_\theta(r,\theta)=\frac{\mu_o I_p}{2\pi r}(1+\Lambda\varepsilon\cos\theta), \tag{2}$$

components, where I_p is the plasma current and I_φ is the current of the magnetic system, $\varepsilon=r/R_0(r)$ is the inverse aspect ratio, $R_0(r)$ is the position of the center of the magnetic surface with radius r. The Shafranov shift $R_0(r)$ with respect to the center of the outmost magnetic surface of radius a is $\Delta(r)=[R_0^2(a)+(\Lambda+1)(a^2-r^2)]^{1/2}-R_0(a)$. The quantity Λ is determined by the ratio of the plasma pressure to the magnetic pressure of the poloidal field, $\beta_{\rm pol}$, and the internal inductance l_i, i.e., $\Lambda=\beta_{\rm pol}+l_i/2-1$. Let B_t be the toroidal magnetic field at $R=R_0(a)$: $B_t=\mu_0 I_\varphi/2\pi R_0(a)$. The safety factor $q(r)\approx rB_\varphi/RB_\theta$ may be represented by (see Ref. 11)

$$q(r)=\varepsilon^2\frac{I_\varphi}{I_p}\left(1+\frac{1}{2}a_2\varepsilon^2+\frac{3}{8}a_4\varepsilon^4+\cdots\right), \tag{3}$$

where

$$a_m=(-1)^m\sum_{k=0}^{m}(m-k+1)\Lambda^k.$$

The presented model well describes the magnetic equilibrium at the plasma edge.

Divertor coil configuration: As in Refs. 11 and 12 we consider the ideal divertor coil configuration in which 16 identical helical conductors located on the inboard circumference of radius r_c and uniformly distributed along the **B**. The poloidal extension of coils is $\Delta\theta=2\theta_c=\pi/5$. The current distribution on the coils is taken as $I_j=ccI_d\sin(\pi j/2+\omega t)$, where j $(j=1,\ldots,16)$ stands for a coil number, cc is the current control factor $(0\leqslant cc\leqslant 1)$, $I_d=15$ kA is the maximum possible current, ω is a rotation frequency of the perturbation field. This current distribution creates magnetic perturbations at the plasma edge with the toroidal mode $n=4$ possessing a strong radial decay $\sim(r/r_c)^{m_0-1}$ $(m_0=20)$.

The divertor target plates are located at $r=r_d<r_c$ at the HSF. Tracing field lines are terminated when field lines hit the divertor plate. For the DED of TEXTOR the position of the divertor plates is taken at $r_d=49$ cm.

III. HAMILTONIAN FIELD LINE EQUATIONS

The magnetic structure at the plasma boundary is studied by integrating the field line equations given in Hamiltonian form,

$$\frac{d\theta^*}{d\varphi}=\frac{\partial H}{\partial\psi},\quad \frac{d\psi}{d\varphi}=-\frac{\partial H}{\partial\theta^*}, \tag{4}$$

with the poloidal flux H as a Hamiltonian function $H=\psi_p(\theta^*,\psi,\varphi)$, a toroidal flux ψ and an intrinsic poloidal coordinate θ^* as the canonical variables $(\psi=\psi(r),\theta^*=\theta^*(r,\theta))$, and the toroidal angle φ as an independent time-like variable. [In the intrinsic coordinates (θ^*,ψ) field lines on the given magnetic surface $\psi=$const are straight in the absence of a perturbation, $\theta^*=\theta_0^*+(\varphi-\varphi_0)/q(\psi)$.]

For the equilibrium magnetic field (1), (2) and the ideal divertor coil configuration the Hamiltonian function H is found in Ref. 11, and it has the form,

$$H=H_0(\psi)+\epsilon H_1(\theta^*,\psi,\varphi),$$

$$H_0(\psi)=\int\frac{d\psi}{q(r(\psi))}, \tag{5}$$

$$H_1(\theta^*,\psi,\varphi)=\sum_m H_m(\psi)\cos(m\theta^*-n\varphi+\omega t),$$

where the dimensionless perturbation parameter $\epsilon = B_d/B_t$ is the ratio of the magnetic perturbation amplitude $B_d = \mu_o I_d n/\theta_c r_c$ to the toroidal field B_t at the magnetic axis. The perturbed part of the poloidal flux $H_1(\theta^*,\psi,\varphi)$ has the following asymptotic representation for its Fourier components $H_m(\psi)$ (for large poloidal numbers m):

$$H_m(\psi) = (-1)^{m+m_0} C \frac{\sqrt{R_0(R_0-r)}}{R_0^2} \left(\frac{r-\Delta(r)}{r_c}\right)^{m^*} \times \frac{\sin(m^*-m)\theta_c}{\pi\beta_1 m^*(m^*-m)}, \tag{6}$$

where

$$m^* = \frac{m + x_c(m\beta_3/2\beta_1)^{1/3}}{\beta_1}.$$

The parameters β_1 and β_3 are the first and third derivatives of the poloidal angle θ with respect to the intrinsic angle θ^* taken at the HFS, i.e.,

$$\beta_1 = \left.\frac{d\theta}{d\theta^*}\right|_{\theta=\pi}, \quad \beta_3 = \left.\frac{d^3\theta}{d\theta^{*3}}\right|_{\theta=\pi}.$$

In Eq. (6) there are two parameters C and x_c determined by fitting the asymptotic formula (6) with the direct numerical calculations (see Ref. 11). These parameters weakly depend on the plasma parameter $\beta_{\rm pol}$ and take values in the interval, $1<C<1.055$, $-0.23<x_c<-0.36$.

A. Mapping method of integration of field line equations

The field lines may be studied by direct integration of the Hamiltonian equations (4). However, it requires rather long computation times. Replacing the Hamiltonian system by a mapping would significantly simplify speed up these calculations.

Below we study the Hamiltonian field line equations using a symplectic mapping procedure. It is a generalization of the new integration method of Hamiltonian systems, recently developed in Refs. 18,11, to smaller integration steps. It is much more accurate than the original scheme, and allows one to consider the cases with moderately high perturbations. In particular, it allowed us to study field lines at the laminar zone of the DED where the perturbation field is sufficiently large, i.e., when the perturbation parameter ϵ is not small and has the order of $\epsilon \sim 0.1-0.2$. The method is based on a canonical change of variables that eliminates the perturbation during periodic time intervals. This procedure allows one to reduce the continuous Hamiltonian equations to a symplectic mapping. Details of this method will be published elsewhere.

The magnetic perturbation (5) has an n-fold symmetry along the toroidal axis, i.e., it is a periodical function of the toroidal angle φ with the period $2\pi/n$. We introduce poloidal sections at $\varphi = \varphi_k = (2\pi/ns)k$ $(k = 0, \pm 1, \pm 2, \ldots)$, where $s \geqslant 1$ is an integer number. Note that the sections φ_k and φ_{k+ns} coincide. Let (ψ_k, θ_k) be intersection points of the field line with the poloidal section $\varphi = \varphi_k$. We define a forward map as

$$(\psi_{k+1}, \theta^*_{k+1}) = \hat{T}_f(\psi_k, \theta^*_k). \tag{7}$$

Similarly, one can define a backward map

$$(\psi_{k-1}, \theta^*_{k-1}) = \hat{T}_b(\psi_k, \theta^*_k). \tag{8}$$

Note that the Poincaré map may be obtained by applying the maps (7), (8) s times, i.e., $(\hat{T}_f)^s$. In Refs. 18 and 11 the integration step $\Delta\varphi$ was taken to equal to the period of the perturbation $2\pi/n$. Here we construct the symplectic maps for smaller steps $\Delta\varphi = 2\pi/ns$ $(s \geqslant 1)$.

The mappings (7), (8) are constructed by combining three symplectic maps $\hat{T}_-(\varphi)$, $\hat{T}_0(\varphi',\varphi)$, and $\hat{T}_+(\varphi)$. The maps $\hat{T}_-(\varphi)$, $\hat{T}_+(\varphi)$ perform a canonical change of variables in the Hamiltonian equations. They are implemented by the generating function $F(\bar{\psi},\theta^*,\varphi) = \bar{\psi}\theta^* + S(\bar{\psi},\theta^*,\varphi)$. In particular, the map $\hat{T}_+$: $(\bar{\psi},\bar{\theta}^*) = \hat{T}_+(\varphi)(\psi,\theta^*)$ transforms the original variables (ψ,θ^*) to the new ones $(\bar{\psi},\bar{\theta}^*)$ at a fixed value of the toroidal angle φ, i.e.,

$$\bar{\psi} = \psi - \epsilon \frac{\partial S(\bar{\psi},\theta^*,\varphi)}{\partial\theta^*}, \quad \bar{\theta}^* = \theta^* + \epsilon \frac{\partial S(\bar{\psi},\theta^*,\varphi)}{\partial\bar{\psi}}, \tag{9}$$

thereby transforming the Hamiltonian (5) H to a new one $\mathcal{H}$

$$\mathcal{H} = \mathcal{H}_0(\bar{\psi},\epsilon) + \epsilon\mathcal{H}_1(\bar{\theta}^*,\bar{\psi},\varphi,\epsilon),$$
$$\mathcal{H}_1(\bar{\theta}^*,\bar{\psi},\varphi,\epsilon) = \mathcal{H}_1(\bar{\theta}^*,\bar{\psi},\epsilon)\sum_{k=-\infty}^{\infty}\delta\left(\varphi - \frac{2\pi}{ns}\right), \tag{10}$$

with no perturbations in a toroidal section $\varphi_k < \varphi < \varphi_{k+1}$, while the map $\hat{T}_-(\varphi)$ creates out the inverse transformation of variables $(\psi,\theta^*) = \hat{T}_-(\varphi)(\bar{\psi},\bar{\theta}^*)$,

$$\psi = \bar{\psi} + \epsilon \frac{\partial S(\bar{\psi},\theta^*,\varphi)}{\partial\theta^*}, \quad \theta^* = \bar{\theta}^* - \epsilon \frac{\partial S(\bar{\psi},\theta^*,\varphi)}{\partial\bar{\psi}}. \tag{11}$$

The map $\hat{T}_0(\varphi',\varphi)$: $(\bar{\psi}',\bar{\theta}^{*\prime}) = \hat{T}_0(\varphi',\varphi)(\bar{\psi},\bar{\theta}^*)$ describes the evolution of the new variables $(\bar{\psi},\bar{\theta}^*)$ in the unperturbed system between φ and φ' (both in the interval $\varphi_k < \varphi,\varphi' < \varphi_{k+1}$), i.e.,

$$\bar{\psi}' = \bar{\psi}, \quad \bar{\theta}^{*\prime} = \bar{\theta}^* + \frac{\varphi'-\varphi}{\bar{q}(\bar{\psi})}, \tag{12}$$

where

$$\frac{1}{\bar{q}(\psi,\epsilon)} = \frac{\partial\mathcal{H}_0(\psi,\epsilon)}{\partial\psi} \tag{13}$$

is the safety factor in the new variables.

According to (9), (11), and (12) the forward map (7) may be constructed as a sequence of the maps $\hat{T}_+(\varphi_k)$, $\hat{T}_0(\varphi_{k+1},\varphi_k)$ and $\hat{T}_-(\varphi_{k+1})$, respectively, i.e.,

$$(\psi_{k+1},\theta^*_{k+1})=\hat{T}_f(\psi_k,\theta^*_k)$$
$$=\hat{T}_-(\varphi_{k+1})\hat{T}_0(\varphi_{k+1},\varphi_k)\hat{T}_+(\varphi_k)$$
$$\times(\psi_k,\theta^*_k). \tag{14}$$

Similarly the backward map (8) may be represented by

$$(\psi_{k-1},\theta^*_{k-1})=\hat{T}_b(\psi_k,\theta^*_k)$$
$$=\hat{T}_-(\varphi_{k-1})\hat{T}_0(\varphi_{k-1},\varphi_k)\hat{T}_+(\varphi_k)$$
$$\times(\psi_k,\theta^*_k). \tag{15}$$

The mappings (14)–(15) are invariant with respect to the transformation $k\leftrightarrow k+1$.

B. The generating function

In general the generating function $S(\psi,\theta,\varphi)$ satisfies the Hamilton–Jacobi equation

$$\mathcal{H}\left(\bar{\psi},\theta^*+\epsilon\frac{\partial S}{\partial\bar{\psi}},\varphi\right)=H\left(\bar{\psi}+\epsilon\frac{\partial S}{\partial\theta^*},\theta^*,\varphi\right)+\frac{\partial S}{\partial\varphi}. \tag{16}$$

Solving this equation for an arbitrary perturbation parameter ϵ is a very difficult task. For the small perturbation it may be sought using perturbation theory expansion (16) and $S(\psi,\theta,\varphi)$ taking a series in powers in ϵ (Ref. 18). Below we present its solution to first order of ϵ. As was shown in Refs. 11 and 18 the mapping (14) with such a solution for the generating function S well reproduces the orbits of Hamiltonian equations (4) obtained by the numerical symplectic integration scheme.

Suppose that the perturbed Hamiltonian has the Fourier expansion (5), then the generating function $S(\psi,\theta,\varphi)$ to the first order of perturbation theory may be written in the form of a Fourier series

$$S(\psi,\theta,\varphi)=\sum_m\{S^{(s)}_m(\psi)\sin(m\theta^*-n\varphi)$$
$$+S^{(c)}_m(\psi)\cos(m\theta^*-n\varphi)\}, \tag{17}$$

with angle-dependent coefficients,

$$S^{(s)}_m(\psi,\varphi)=-H_m(\psi)\frac{\pi}{n}\frac{1-\cos(\alpha_m(\psi)[n\varphi/\pi])}{\alpha_m(\psi)},$$
$$S^{(c)}_m(\psi,\varphi)=H_m(\psi)\frac{\pi}{n}\frac{\sin(\alpha_m(\psi)[n\varphi/\pi])}{\alpha_m(\psi)}, \tag{18}$$

where $[n\varphi/\pi]=(2k+1)/s-n\varphi/\pi$, for $\varphi_k<\varphi<\varphi_{k+1}$, and

$$\alpha_m(\psi)=\frac{\pi}{n}\left(\frac{m}{q(\psi)}-n\right).$$

The coefficient $S^{(c)}_m(\psi,\varphi)$ in (18) is a discontinuous function of φ at the values $\varphi=\varphi_k$. At the limit $\varphi\to\varphi_k\pm 0$ we have

$$S^{(c)}_m(\psi,\varphi_k\pm 0)=\pm H_m(\psi)\frac{\pi}{n}\frac{\sin\alpha_m(\psi)}{\alpha_m(\psi)}. \tag{19}$$

In the next section the symplectic maps (14)–(15) are applied to study the ergodic and laminar zones of the DED. To study Poincaré sections we have chosen the integration step $\Delta\varphi$ equal to the period of the perturbation $2\pi/n$. To obtain the laminar plots one needs the higher accuracy of calculation. For this case the integration step $\Delta\varphi$ is taken eight times smaller, i.e., $\Delta\varphi=2\pi/ns$ $(s=8)$.

IV. STRUCTURES OF THE ERGODIC AND THE LAMINAR ZONES

A. Formation of the ergodic and the laminar zones

The poloidal spectrum H_m (6) of the magnetic perturbation is located near the central poloidal mode $m_c\approx m_0\beta_1$ with the width $\Delta m\approx\pi\beta_1/\Delta\theta$ (see Ref. 11). In general m_c and Δm depend on the plasma parameter $\beta_{\rm pol}$ as well as on the radial coordinate r. For the standard operational regime $(\beta_{\rm pol}=1)$ the DED perturbation coils are designed to create the ergodic zone at the plasma edge near the magnetic surface $q=3$ located near $r=43$ cm. It is expected that one can obtain the well-developed ergodic zone if $m_c=12$ at the resonant magnetic surfaces $q(r_{mn})=m_c/n=3$. Qualitatively, the mechanism to form the ergodic zone at the plasma edge is the following. The resonant magnetic perturbations with (6) $m_c-\Delta m/2<m<m_c+\Delta m/2$ generate a chain of islands. At a certain level of the perturbed field the interactions of these islands creates the ergodic zone of field lines at the plasma edge. The structure of the ergodic zone depends not only on the mutual positions of the main resonant magnetic surfaces r_{mn} $(m_c-\Delta m/2<m<m_c+\Delta m/2)$ but also on how close they are to the divertor coils at $r=r_c$, this is, because of the strong radial dependence of the magnetic perturbation (6). By outward shift of the main resonant magnetic surfaces r_{mn} one can increase the interaction of resonant islands, and therefore the ergodization level. However, if the perturbation amplitude H_m of the outermost resonant magnetic surface r_{mn} is a sufficiently large it creates a bump on the outside of the island whereby it touches the divertor plate. This island dominates over the inner islands and forms the region with the regular behavior of field lines at the plasma edge. This phenomenon is partly responsible for the formation of the laminar zone. Below we study the formation of the ergodic and the laminar zones more rigorously by plotting Poincaré sections and contour plots of field lines with different poloidal turns (see Sec. V).

B. Variation options of the operational regimes

There are several options to vary the operational regimes of the DED. The first of them is a variation of the divertor current I_d, thereby enhancing the degree of ergodization. However, this may not be sufficient to get a sizeable zone of chaotic field lines, especially for the higher $\beta_{\rm pol}\geqslant 1$ (see Ref. 12). The ergodization level of field lines may be increased by lowering $\beta_{\rm pol}$ (Refs. 11 and 12), however, this option is not desirable.

The most convenient way to regulate the degree of ergodization and the width of the ergodic layer is a variation of the radial positions of the main resonant magnetic surfaces $r=r_{mn}$, where $q(r_{mn})=m/n$. The shift $r=r_{mn}$ with respect to the DED-coils may be accomplished, according to (3), by varying the plasma current I_p or the toroidal magnetic field

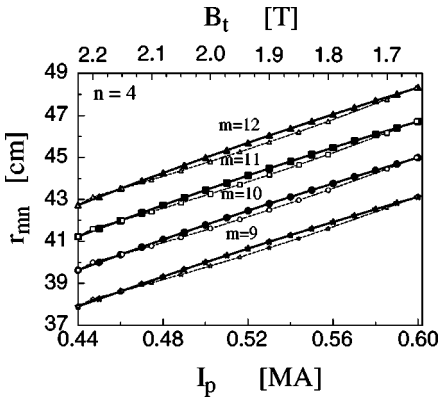

FIG. 1. Radial positions of the resonant magnetic surfaces r_{mn} vs the plasma current I_p at a fixed toroidal magnetic field $B_t=2.25$ T (solid curves) and vs the toroidal magnetic field B_t at the plasma current $I_p=0.44$ MA (dashed curves).

B_t (through the main current of the magnetic system I_φ). At the fixed value of I_φ the positions of the resonant magnetic surfaces r_{mn} increase approximately linearly with the plasma current I_p: $r_{mn}=r^0_{mn}+r'_{mn}I_p$. For the equilibrium plasma parameters $a=46$ cm, $R_0=174$ cm, $\beta_{\rm pol}=1.0$, the dependencies of r_{mn} on the plasma current I_p at the fixed toroidal magnetic field $B_t=2.25$ T (solid curves) and on the magnetic field B_t at the fixed plasma current $I_p=440$ kA (dashed curves) are shown in Fig. 1 for the main poloidal modes $m=9$, 10, 11, 12. The parameters r^0_{mn} and r'_{mn} are equal to $r^0_{mn}=24.99$ cm, $r'_{mn}=3.35\times10^{-2}$ $(\mathrm{kA})^{-1}$ for the resonance $m{:}n=10{:}4$; $r^0_{mn}=26.25$ cm, $r'_{mn}=3.43\times10^{-2}$ $(\mathrm{kA})^{-1}$ for $m{:}n=11{:}4$, and $r^0_{mn}=27.45$ cm, $r'_{mn}=3.50\times10^{-2}$ $(\mathrm{kA})^{-1}$ for $m{:}n=12{:}4$. For example, the resonant surface $r_{m,n}$ $(m=12,n=4)$ changes from 42.73 cm to 48.33 cm when I_p is increased from 440 kA to 600 kA (at the fixed $B_t=2.25$) or B_t is decreased from 2.25 T to 1.65 T (at the fixed $I_p=440$ kA).

Below we study the variation of the plasma regimes at the different values of the plasma current I_p keeping the magnetic field B_t fixed. The changes of the plasma regime can be also produced by varying the magnetic field B_t at the fixed plasma current. However, one should note that for the two magnetic equilibria $(I^{(1)}_p,B^{(1)}_t)$, $(I^{(2)}_p,B^{(2)}_t)$ which have the same resonant magnetic surfaces r_{mn}, the plasma edge will be affected more strongly in the case with the smaller toroidal magnetic field $B_t=\min(B^{(1)}_t,B^{(2)}_t)$. It is due to the fact that the relative magnetic perturbation ϵ in the field line Eqs. (4), (5) is inversely proportional to the toroidal magnetic field B_t.

C. Poincaré sections

We plotted Poincaré sections of field lines by iterating the forward map (14) for different plasma currents I_p. The Poincaré section of field lines at the poloidal plane $\varphi=$const is shown in Fig. 2 for the plasma current $I_p=480$ kA and the maximum divertor current $I_d=15$ kA. Other parameters taken are $B_t=2.25$ T, $a=46$ cm, $R_0=174$ cm and $\beta_{\rm pol}=1.0$. Figure 2(a) shows the entire poloidal section in the polar coordinate system (θ,ρ), centered at the center of the

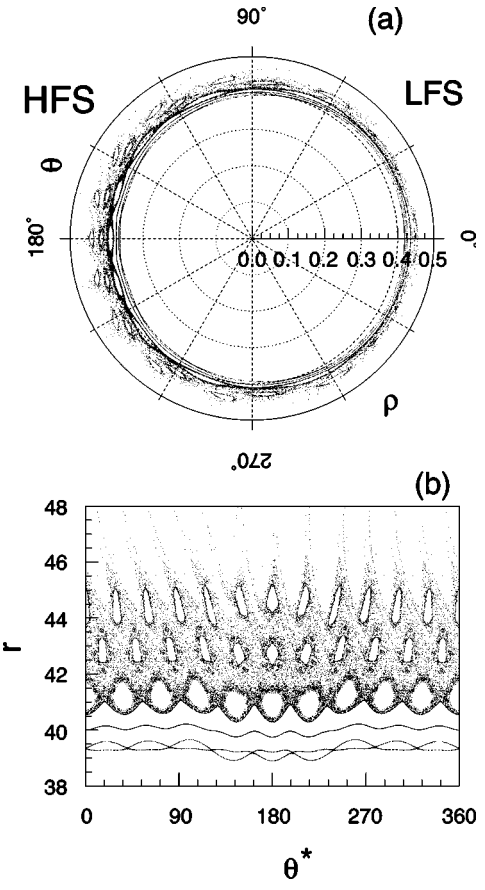

FIG. 2. Poincaré sections of magnetic field lines: (a) in a polar coordinate system (r,θ); (b) close up view of the ergodic zone; $I_p=480$ kA.

last magnetic surface of radius $r=a$ while the close up view of the plot at the plasma edge is shown in Fig. 2(b) in the (θ^*,r)-plane, where r is a radial distance from the magnetic axis.

The width of the ergodic zone, formed at the plasma boundary, is wider at the HSF than at the low field side (LFS). From Fig. 2(b) one can see that the magnetic field structure at the plasma boundary may be divided into two distinct zones: the ergodic zone $(r_{\rm LMS}<r<r_l\approx46$ cm) with well developed chaotic field lines (containing embedded islands of regular field lines) and the laminar zone $(r_l<r<r_d=49$ cm) with open field lines connecting to the divertor target on both sides. Here $r_{\rm LMS}$ stands for the last conserved magnetic surface. The ergodic zone is connected with the divertor target plates along narrow chaotic stripes. The large white areas between these chaotic stripes in the laminar zone correspond to the field lines with relatively short connection lengths (one or a few poloidal turns). (They do not appear in a Poincaré plot.) The radial distance r_l defines the boundary between the ergodic zone and the laminar zone. The widths of the ergodic zone and the laminar zone can be changed by varying the divertor current cc or by shifting the resonant magnetic surface in the radial direction by varying the plasma current I_p. Below we consider the effect of the variation of the plasma current on the ergodic and the laminar zones.

At the plasma current $I_p=480$ kA the width of the er-

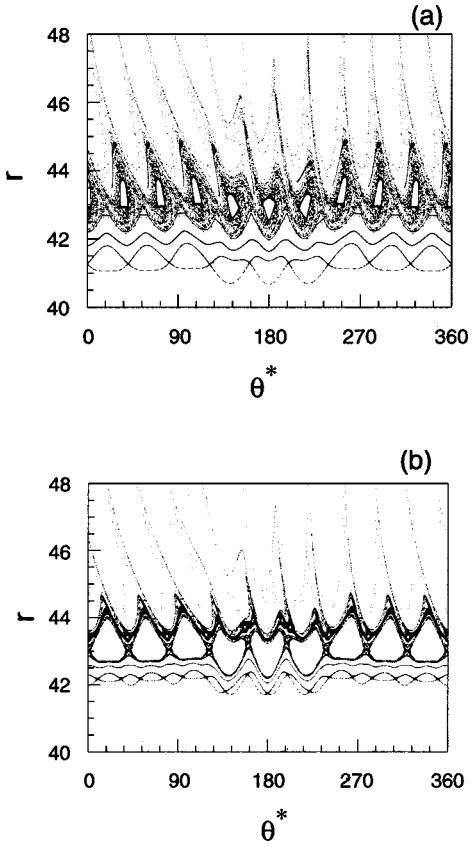

FIG. 3. Poincaré sections of magnetic field lines for different poloidal currents: (a) $I_p=540$ kA; (b) $I_p=600$ kA. Other parameters are the same as in Fig. 2.

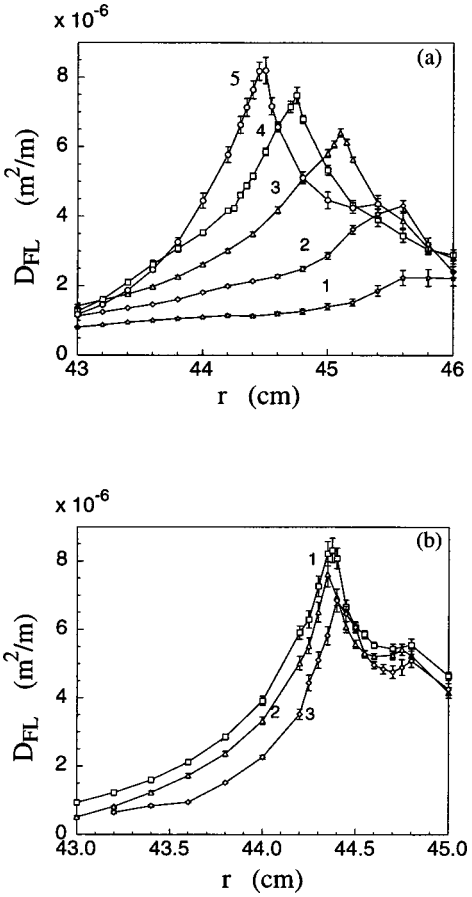

FIG. 4. Profiles of field line diffusion coefficients $D_{\mathrm{FL}}(r)$ for different poloidal currents: (a) curve 1, $I_p=460$ kA; 2, $I_p=480$ kA; 3, $I_p=500$ kA; 4, $I_p=520$ kA; 5, $I_p=540$ kA; (b) 1, $I_p=560$ kA; 2, $I_p=580$ kA; 3, $I_p=600$ kA. The other parameters are the same as in Fig. 2.

godic zone is relatively large (about $\Delta r\approx 5$ cm) [see Fig. 2(b)]. The increase of I_p shifts outward the positions r_{mn} of the resonant magnetic surfaces. Due to the strong radial dependence of perturbation (6) the widths of individual islands grow further thereby enhancing their interaction. It leads to a widening of the laminar zone and narrowing of the ergodic zone; this is because of the dominance of the resonant mode being closely located to the divertor coils and by diminishing of the contributions of resonant modes m far from the central mode m_0 (6). Figure 3 shows the structure of field lines at the plasma boundary for two values of the plasma current: (a) $I_p=540$ kA; (b) $I_p=600$ kA. The width of the ergodic zone is substantially decreased (approximately from 5 cm to 2 cm) when the plasma current is varied from 480 kA to 540 kA, while the width of the laminar zone is increased by only approximately 2 cm [compare Figs. 2(b) and 3(a)]. Further increase of I_p up to 600 kA leaves a narrow ergodic layer without noticeable change of the width of the laminar zone.

D. Field line diffusion coefficients

The variation of the ergodic and laminar zones may also be studied by the radial field line diffusivity. In order to study the field line diffusion we have calculated by the second-order radial displacement moments,

$$\sigma_{r_0}(l)=\langle (r(l)-r_0)^2\rangle,$$

averaged over a set of field lines with initial angle θ^* being uniformly distributed in the poloidal plane at a fixed minor radius r_0. Here l is the distance along field lines. In the ergodic zone $\sigma_{r_0}(l)$ typically grows with the distance l up to a certain distance then it converges to a constant value in case field lines are confined in the ergodic zone, or it decreases exponentially when the field lines leave the ergodic zone after reaching the divertor plate. In general, it is not possible to introduce a global diffusion coefficient $D=\sigma_{r_0}(l)/2l$ for the limit $l\to\infty$ within a finite ergodic zone, as it is possible in the unlimited domain. However, in order to estimate the radial stochastic transport rate of field lines, one can introduce a local diffusion coefficient $D_{\mathrm{FL}}(r_0)$ valid for the initial linear growth of $\sigma_{r_0}(l)$ with l, i.e., $\sigma_{r_0}(l)=2D_{\mathrm{FL}}(r_0)l$ (see Ref. 11).

Profiles of $D_{\mathrm{FL}}(r)$ are presented in Fig. 4 for the different plasma currents. In the ergodic zone ($r<r_l$) D_{FL} grows monotonically up to the boundary of the laminar zone r_l then it decreases for $r>r_l$ despite the growing perturbation. The width of the laminar zone also increases with the plasma current I_p up to the value of 540 kA. For the higher values of $I_p>540$ kA the laminar zone stagnates. Similarly D_{FL} in the ergodic zone does also grow with I_p up to the same value 540 kA, but for $I_p>540$ kA it slightly decreases. This de-

crease in the diffusion rate within the laminar zone is due to a drastic reduction of the contribution of chaotic field lines to the diffusion process, and dominating the convective field lines (connecting the divertor plates with themselves in a few poloidal turns) on the transport of heat and particles.

V. FRACTAL STRUCTURE OF THE LAMINAR ZONE

A. Ergodic divertor as an chaotic scattering system

Field lines at the plasma edge with initial coordinates located outside the last invariant magnetic surface eventually leave the plasma region along the torus reaching the wall in both, clockwise and counterclockwise directions (expect for those field lines being trapped inside the magnetic islands). In this sense such a system may be viewed as one of chaotic scattering, whereby field lines enter into the plasma edge from the wall and leave when hitting the wall after a certain number toroidal (or poloidal) turns. Indeed, field lines may enter into (or leave) the plasma edge only from some thin areas on the wall known as *magnetic footprints* (see Refs. 23,26,27,9). The length of these field lines inside the plasma region is very sensitive to their initial coordinates within these areas: a tiny change of the input conditions can produce drastic changes in the length of field lines.

In chaotic scattering systems, a trajectory may leave the system in one of several different ways. The space of initial coordinates corresponding to the various exit ways are separated by a boundary, which may be a fractal (Ref. 30). The set of initial conditions for which trajectories leave the system in a particular way is called the basin of the particular mode. In the case of the ergodic divertor it is convenient to classify the field lines by the number of poloidal turns, i.e., by the numbers of rotation around the minor cycle. Indeed, the perturbation field of divertor coils are highly localized on the HFS, and field lines enter into the plasma and leave it on this side making almost full poloidal turns. Therefore, the set of initial conditions for which field lines crossing the equatorial plane on the LFS with the same number of times may be referred as the basin of a particular number of poloidal turns N_p. Spatial structures of boundaries of basins belonging to the different N_p give a fine details of the ergodic and laminar zone which cannot be revealed by Poincaré sections. Below we study such structures of the laminar zone by plotting the contours of N_p within the plasma edge and on the divertor plate.

One should note that the contour plots similar to these, called laminar plots, were first introduced in Refs. 6 and 8, where the lengths of field lines were used instead of N_p.

B. Basin boundary structure at the plasma edge

In this and the next subsections we study the basin boundary structure at the plasma edge and on the wall, respectively. For the first case, unlike the definition given above, we will refer to the basin as a set of spatial points (θ^*,r) at the given poloidal section $\varphi=$const which are crossed by field lines connecting wall to wall with a particular number of poloidal turns N_p. The entire plot showing the boundaries between basins with different numbers of poloidal turns may give more details about the laminar zone than Poincare sections. The procedure to obtain these plots is the following.

At the poloidal plane $\varphi=0$ the field line with a given initial coordinate (θ^*,r) is traced along the positive direction of φ by iterating the forward map (7) and in the negative direction using the backward map (8) until the field line reaches the divertor plate. Then we determine a fractional number of poloidal turns $N_{\rm pol}$ as the ratio of the total change of the poloidal angle $\Delta\theta^*$ to the full circle 2π, i.e., $N_{\rm pol}=\Delta\theta^*/2\pi$. The values of $N_{\rm pol}$ computed in this way are close to integer numbers although they are not exactly integer. Let N_p be the integer number closest to $N_{\rm pol}$. Areas in the (θ^*,r)-plane with different poloidal turns N_p are topologically different. The dependence of $N_{\rm pol}$ on the initial coordinates (θ^*,r) may be best understood from a contour plot with contour lines separating the basins of different poloidal turns N_p.

Below we present the basin boundary structure at the laminar zone for two different plasma currents, namely, $I_p=480$ kA and 600 kA. As shown in Sec. IV C in the first case the width of the laminar zone is relatively small, whereas for $I_p=600$ kA the laminar zone covers almost the full area of the plasma periphery. The basin plot for $I_p=480$ kA is shown in Fig. 5; (a) shows the plot on the LFS, (b) on the HFS. Similar plots for $I_p=600$ kA are presented in Fig. 6. In these figures the basins corresponding up to six poloidal turns are shown. The darkest blue basin corresponds to field lines with the shortest connection lengths (less than one poloidal turn) and describes the private flux zone. This basin is located on the HFS only where the perturbation coils are positioned. The darkest red area describes the basins with more than six poloidal turns. The boundaries between these basins are not resolved. The basins corresponding to the field lines with N_p ranging from one poloidal turn to six poloidal turns are colored according the color bar in Figs. 5 and 6: the color of the basin N_p is determined by the color at the level $N_p-0.5$ of the color bar.

The basin with one poloidal turn has a nonfractal boundary with the private flux zone. But it may have fractal boundaries with the basins corresponding to two and more poloidal turns. For $N_p\geqslant 2$ there are several topologically different basins related to the same N_p. As see from Figs. 5 and 6, the relatively large basins of a few poloidal turns $N_p\leqslant 3$ at the plasma edge are clearly separated by nonfractal boundaries. But they are alternating with the long dark elongated areas (or stripes) containing the basins for a few poloidal turns up to very large N_p. The increase of the plasma current I_p to 600 kA leads not only to a radial expansion of the basins with a few poloidal turns but also to a growth of the number of stripes. In Ref. 15 these stripes have been called ''fingers.'' At the HFS some of these stripes are radially extended toward the wall (divertor plate).

The structure of the stripes has a complicated fractal nature. In order to study, it we have magnified the area of the stripe with the fine resolution of basins of higher poloidal turns. Figure 7(a) shows a blow up of the yellow rectangle area at the stripe in Fig. 5(b). Further expansion of the yel-

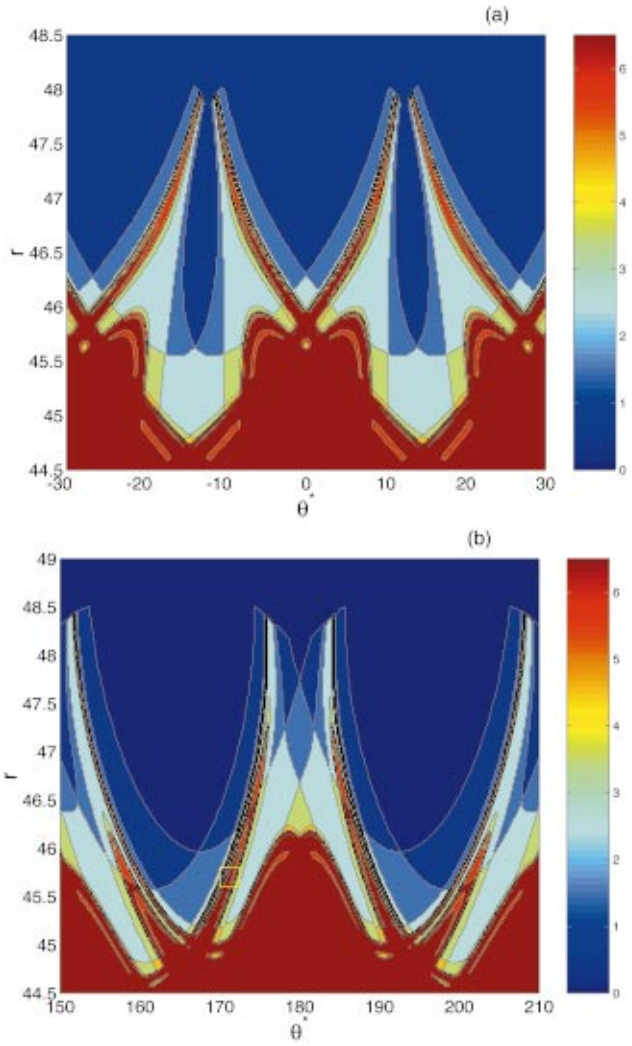

FIG. 5. (Color) Contour plots of N_p in the (θ^*,r)-plane for the plasma currents $I_p=480$ kA. (a) shows the LFS, (b) HFS. The other parameters are the same as in Fig. 2.

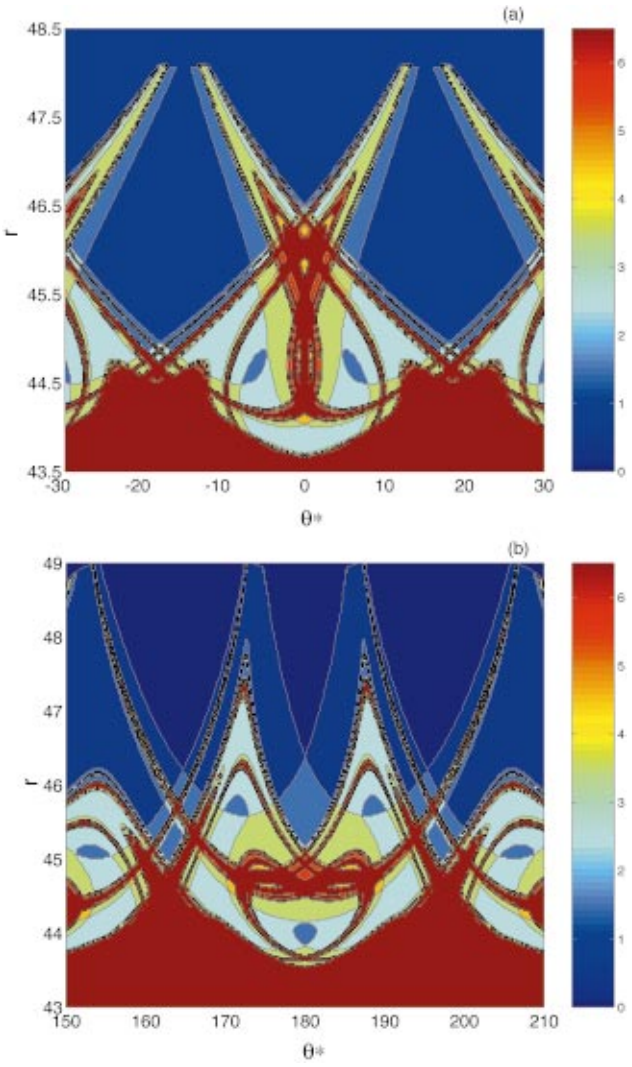

FIG. 6. (Color) Same as in Fig. 5, for the plasma current $I_p=600$ kA. (a) LFS; (b) HFS.

low rectangular region in Fig. 7 is presented in Fig. 7(b). It shows that the basins at the stripe are highly elongated and the boundaries between them have fractal structure, i.e., the stripes consist of layered basins of different poloidal turns with a self-similar behavior at different spatial scales. As seen, the basins of field lines with a few poloidal turns N_p are ''sandwiched'' between basins for field lines with large numbers of poloidal turns $N_p \gg 1$.

C. Magnetic footprints

In order to study the basin boundary structure on the plasma wall we will use the following procedure. We follow a field line which enters into the plasma starting from the wall of radius r_d with the given initial coordinate (φ,θ) and returns back to the wall after a certain number of poloidal turns N_{pol}. The set of initial conditions (φ,θ) with a particular number N_{pol} determines a basin. The whole picture of basin boundaries with $N_{\mathrm{pol}} \geqslant 1$ on the plasma wall determines a structure known as magnetic footprints. Similar to the stripe at the plasma edge the magnetic footprints have a fractal structure as well. Below we consider the structure of magnetic footprints for the above plasma parameters. They are shown in Fig. 8 for the plasma current $I_p=480$ kA and in Fig. 9 for $I_p=600$ kA, particularly, Fig. 8(a) presents magnetic footprints on the entire poloidal region, and Figs. 8(b) and 9(a) show them on the HFS. Finally Figs. 9(b) and 9(c) show the expanded views of the rectangular regions in Fig. 9(a), respectively. Because of the four-fold symmetry along the toroidal direction only one quarter of the magnetic footprints are presented.

One can see from Figs. 8 and 9(a) that the field lines can enter into the plasma (or hit the wall from the plasma side) only along the four pairs of narrow helical stripes. (Dark blue areas in figures correspond to the field lines in a private flux zone.) The distance between stripes of each pairs depends on the plasma current. It is increased with the plasma current and consistent with the consideration of a helical field divertor studied in Ref. 31. Each helical stripe has a fractal structure and it consists of layered basins of different poloidal turns [see Figs. 9(b) and 9(c)]. The width of layers is changing along the toroidal direction φ. The area of the basin with one poloidal turn $N_{\mathrm{pol}}=1$ is the largest. For the

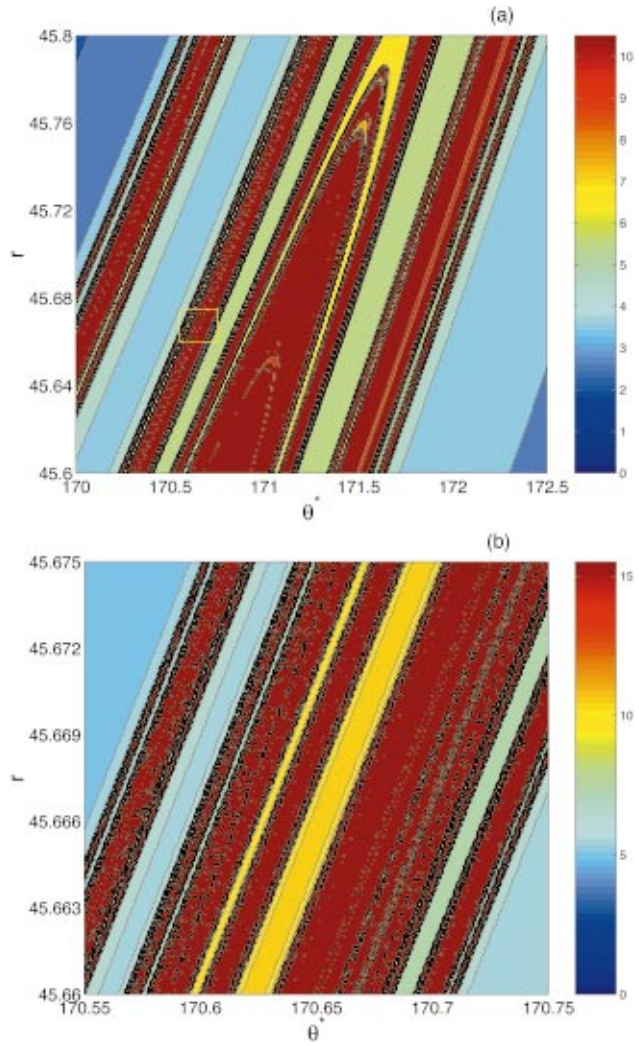

FIG. 7. (Color) (a) Expanded view of the area near the chaotic stripe shown in Fig. 5. (b) Expansion of the rectangular area in Fig. 7(a).

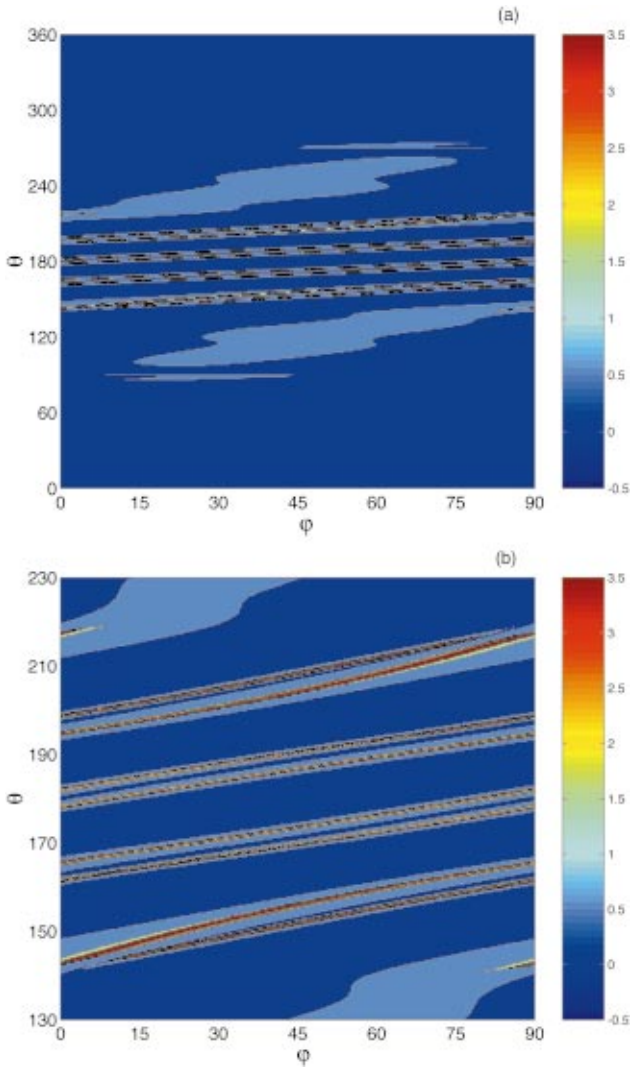

FIG. 8. (Color) Basin boundary structure (magnetic footprints) on the (φ,θ)-plane at the plasma wall $r_d=49$ cm. (a) On the entire plane; (b) close-up view of the HFS. $I_p=480$ kA. The other parameters are the same as in Fig. 2.

higher $N_{\mathrm{pol}}>1$ corresponding areas of basins are drastically decreased in size. The boundaries between these basins are fractal.

The fine structure of the helical stripes can be revealed by studying the dependence of N_{pol} on the poloidal angle θ for fixed toroidal angle φ. Such a dependence of N_{pol} on θ is described by Cantor-type, fractal curves. It is presented in Fig. 10 for the plasma current $I_p=600$ kA at the fixed toroidal angle $\varphi=52°$. The curve in Fig. 10(a) describes the poloidal section of the whole helical stripe shown in Fig. 9(c), while the expanded view of the part of the stripe corresponding to the basins of the large number of poloidal turns $N_{\mathrm{pol}}\gg 1$ are shown in Fig. 10(b). They clearly show areas of field lines connecting wall to wall in one, two, three, and more poloidal turns N_{pol}. These areas are described by almost horizontal steps in the fractal curve. The width of the layer becomes smaller with increasing N_{pol}.

The structure of the helical stripes plays an important role for heat and particle deposition on the divertor plates. Indeed, the basins with $N_{\mathrm{pol}}\gg 1$ correspond to the field lines coming from deep within ergodic zone. These field lines may bring high energetic particles to the wall because the particles predominantly move along field lines. Therefore one can expect that the spatial distribution of power deposition within the helical stripes will depend on the spatial structure of basins with $N_{\mathrm{pol}}>1$. The cross-field diffusion of particles broadens the spatial distribution of power deposition around the maxima located at the basins corresponding to large number of poloidal turns.

VI. CONCLUSIONS

In summary, we investigated the effect of plasma current variation on the properties of perturbed field lines at the plasma periphery in the DED of TEXTOR. It has been shown that the variation of the plasma current strongly affects the properties of the ergodic and laminar zones. The increase of the plasma current (or the decrease of the toroidal magnetic field) shifts the radial positions of the main resonant magnetic surfaces outward. Because of the strong radial dependence of the external magnetic perturbations this leads to an increase of the laminar zone with short wall to wall

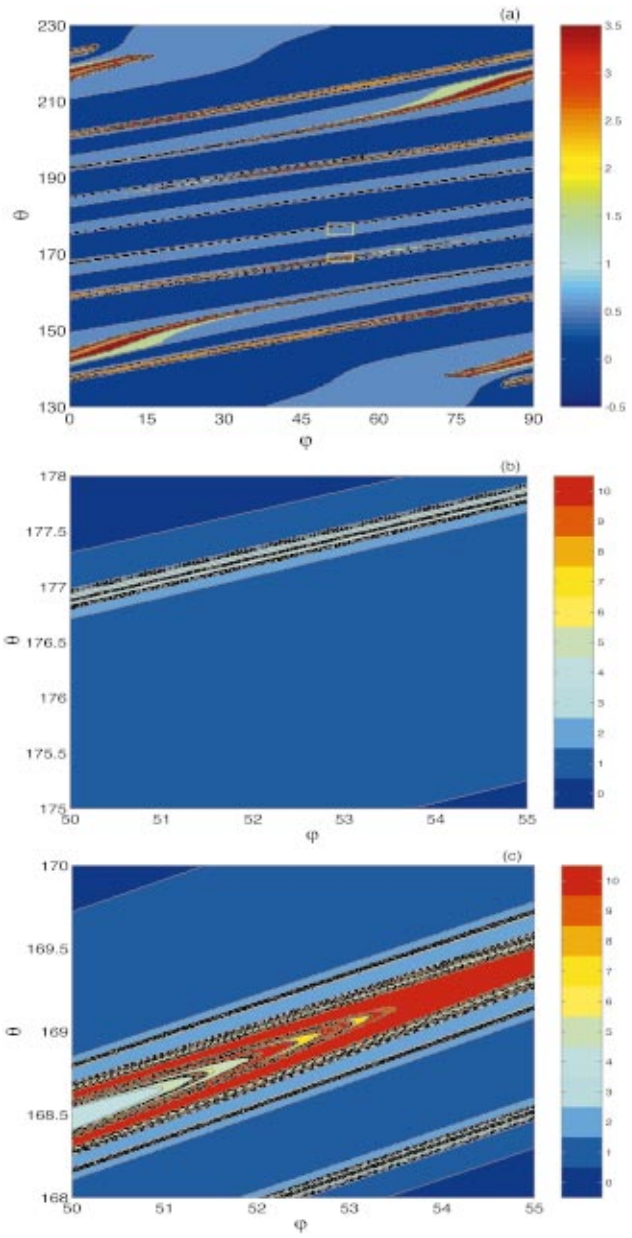

FIG. 9. (Color) Same as in Fig. 8 but for $I_p = 600$ kA. (a) Close-up view of the HFS; (b) expanded view of the upper rectangular region on the stripe shown in (a); (c) the same of the lower rectangular region. Other parameters are the same as in Fig. 6.

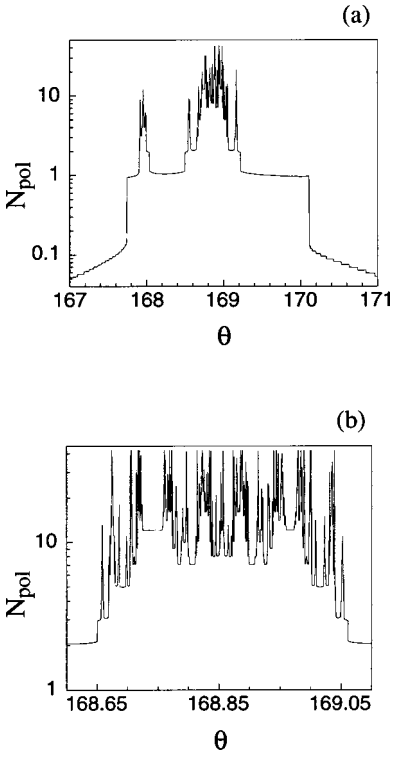

FIG. 10. (a) Fractal dependence of N_{pol} on θ at fixed toroidal angle $\varphi = 52°$ for the plasma currents $I_p = 600$ kA; (b) expanded view of the basins of the large number of poloidal turns. The other parameters are the same as in Fig. 9.

connection lengths of field lines. Variations of the ergodic and laminar zones are also studied by calculating field line diffusivity. In the ergodic zone the field line diffusion coefficients grow monotonically with the radial coordinate, and decrease in the laminar zone. With the increase of the plasma current the radial extend of the growing phase of the diffusion coefficients is narrowed in expense of a widening of their decreasing phase.

The laminar zone consists of clearly separated areas of field lines connecting wall to wall in a few poloidal turns and alternating with narrow long stripe-like areas. We have found that those latter areas have a remarkable fractal structure exposing self-similar and layered areas at different spatial scales. In particular, the number of the wall to wall connecting poloidal turns versus the poloidal angle for fixed minor radius is described by a Cantor-type fractal curve. We have also studied magnetic footprints on the divertor plates. The latter consist of four pairs of helical stripes being consistent with the previous studies. It was found that the each helical stripe has a fractal structure dominantly covered by field lines connecting wall to wall in one poloidal turn. Areas hit by field lines in more than two poloidal turns are drastically reduced. Particularly, field lines coming from deep inside the ergodic zone hit the divertor plate along very narrow Cantor-type fractal stripes.

The study shows the spatial shift of the resonant magnetic surfaces allows to study the transition of plasmas from the regime which has ergodic dominated edge to those similar to normal helical divertor structures.

ACKNOWLEDGMENTS

The authors are grateful to Professor G. Eilenberger and Professor U. Samm for support and interest to the work. They acknowledge stimulating discussions with Dr. G. Fuchs, who thereby gave some suggestions to improve the writing in English.

[1]Dynamic Ergodic Divertor, Special Issue, Fusion Eng. Des. **37**, 335 (1997).
[2]P. Gendrich, A. Grossman, and H. Capes, Plasma Phys. Controlled Fusion **38**, 1653 (1996).
[3]F. Nguyen, P. Gendrich, and A. Grossman, Nucl. Fusion **37**, 743 (1997).
[4]A. Grossman, Plasma Phys. Controlled Fusion **41**, A185 (1999).
[5]A. Kaleck, M. Hassler, and T. Evans, Fusion Eng. Des. **37**, 353 (1997).

[6]K. H. Finken, T. Eich, and A. Kaleck, Nucl. Fusion **38**, 515 (1998).
[7]S. S. Abdullaev, K. H. Finken, and K. H. Spatschek, Phys. Plasmas **5**, 196 (1998).
[8]T. Eich and K. H. Finken, Europhys. Conf. Abstr. **22C**, 1824 (1998).
[9]T. Eich, K. H. Finken, and A. Kaleck, Contrib. Plasma Phys. **38**, 112 (1998).
[10]K. H. Finken, Th. Eich, S. S. Abdullaev *et al.*, J. Nucl. Mater. **266–269**, 495 (1999).
[11]S. S. Abdullaev, K. H. Finken, and K. H. Spatschek, Phys. Plasmas **6**, 153 (1999).
[12]K. H. Finken, S. S. Abdullaev, A. Kaleck, and G. Wolf, Nucl. Fusion **39**, 637 (1999).
[13]M. Hassler, ''Dynamische Ergodisierung für TEXTOR-94,'' Thesis, Institut für Plasmaphysik, Forschungszentrum Jülich, Jülich, 1999, Report No. Jül-3616.
[14]K. H. Finken and T. Eich, Contrib. Plasma Phys. **40**, 57 (2000).
[15]T. Eich, D. Reiser, and K. H. Finken, Nucl. Fusion **40**, 1757 (2000).
[16]T. Eich, D. Reiser, and K. H. Finken, J. Nucl. Mater. **290–293**, 849 (2001).
[17]T. Eich, ''Struktur des Magnetfeldes und des Plasmas in der laminaren Zone des Dynamischen Ergodischen Divertors,'' thesis, Institut für Plasmaphysik, Forschungszentrum Jülich, Jülich, 2000, Report No. Jül-3776.
[18]S. S. Abdullaev, J. Phys. A **32**, 2745 (1999).
[19]B. Eckhard, Physica D **33**, 89 (1988).
[20]S. Bleher, E. Ott, and C. Grebogi, Phys. Rev. Lett. **63**, 919 (1989).
[21]T. Tel and E. Ott, Chaos **3**, 417 (1993).
[22]E. Ott and T. Tel, Chaos **3**, 417 (1993).
[23]N. Pomphrey and A. Reiman, Phys. Fluids B **4**, 938 (1992).
[24]A. Reiman, Phys. Plasmas **3**, 906 (1996).
[25]S. S. Abdullaev and G. M. Zaslavsky, Phys. Plasmas **3**, 516 (1996).
[26]A. Punjabi, A. Verma, and A. Boozer, Phys. Rev. Lett. **69**, 3322 (1992).
[27]A. Punjabi, A. Verma, and A. Boozer, J. Plasma Phys. **52**, 91 (1994); **56**, 569 (1996).
[28]A. Punjabi, H. Ali, and A. Boozer, Phys. Plasmas **4**, 337 (1997).
[29]F. Nguyen, Ph. Ghendrich, and A. Samain, *Calculation of Magnetic Field Line Topology of Ergodized Edge Zone in Real Tokamak Geometry. Application to the Tokamak Tore Supra through the Mastoc Code* (Association Euratom-CEA/Cadarache, 1995), EUR-CEA-FC-1539.
[30]S. Bleher, C. Grebogi, and E. Ott, Physica D **46**, 87 (1990).
[31]K. H. Finken, Nucl. Fusion **37**, 583 (1997).